

Ultrasonic Wave Feature Extraction for Neural Network Classification in not Accessible Pipes

G. ACCIANI, G. BRUNETTI, G. FORNARELLI, C. GUARAGNELLA

Dipartimento di Elettrotecnica ed Elettronica

Politecnico di Bari

Via E. Orabona 4, 70125, Bari

ITALY

Abstract: - The ultrasonic inspection technique can be very useful to determine the state of non reachable structure. In this paper a method based on the neural network classification to evaluate the corrosion level of non accessible pipes is shown. A set of optimal features constitutes the database and feeds the neural network. These features are chosen by time and frequency features extracted from simulated ultrasonic waves. The results show that the method perform a good recognition rate and the different classes are useful for the human decision to evaluate the corrosion level of the pipe under test.

Key-Words: - Ultrasonic waves, Neural networks, k -nearest neighbour, non accessible pipes, feature extraction, non destructive evaluation.

1 Introduction

The non-destructive evaluation (NDE) are used extensively for detection of flaws on non accessible materials and installations. When they resemble a wave guide, for example a thin plate or tube, ultrasonic guided waves can be generated in the structures, so much research has been carried out in the use of guided waves for various NDE application. Ultrasonic based inspection techniques have to obtain the highest possible detection probability and the most exact size, location and type of the defect. The identification of the defect or the knowledge of its nature is very delicate in this technique because the range and variety of imperfections encountered is large, while the quality requirements of new standards is increasing. However, this inspection process may well rely significantly on the skill and experience of an expert. After suitable training the human expert is uniquely able to classify a wide range and variety of complex patterns, even if his performance are subject to significant variation as a result of factors such as fatigue and loss of concentration. For this reason in recent years an huge research effort has been devoted to automate part of the analysis and classification process, in order to improve the overall performance by removing some of burden from the testers [1-9]. Many of these techniques are based on the artificial neural networks and often they are used as classifiers [3-5]. In this paper a neural network approach to support the expert is proposed, offering advantages in terms of improvements in the diagnosis process. The ultrasonic inspection is carried out on non accessible pipes and its aim is to evaluate the corrosion state of the tubes. This problem is wide spread in many industries and involves many different structures and has long been of interest, but is often tedious, time consuming and produce a big burden work for the expert. The ultrasonic waves have good potentiality to overcome these problems, in fact they

have low attenuation and therefore long propagating distances, in this way large area corrosion detection and classification could be possible [2]. Early studies showed the promise of accomplishing this through pattern recognition techniques to classify echoes automatically from their features. The features considered in a commercial package for data analysis based on pattern recognition was used in [8], [9] with the purpose to separate the echoes coming from cracks, counterbore and root waveforms in metal pipes, moreover in [9] a reduction set of those features for ultrasonic testing is reported. These sets allow to separate the waveforms returned at the displacement sensor in various classes related to the possible defect (crack) or geometries (counterbore and root) in the weld of the pipes and plates. This paper presents an automated method to evaluate four different types and configurations of corrosive flaws in metal pipes. The principal goal of this approach is to give class references for the echoes and as a consequence to support the human operator in the evaluation of the size of the corroded part. The method uses the features proposed in [8], [9] added of other two features. The database of this study is constituted with waveforms simulated by software CAPA based on the finite elements technique, whereas the details about the used simulation software parameters or material coefficients are displayed in the following sections of the paper. Time and frequency features have been used to distinguish between echoes from different flaws with known geometries, while the classification k -nearest neighbour algorithm has been employed to select a reduced optimal feature set. This allows the automatic identification of relevant from non-relevant indications that characterize the defect, achieving the feature set that feeds the artificial neural network. The neural network performs the classification of waveforms and distinguish the defects of different dimension. The

results show that four types of flaws are classify correctly with good recognition rate.

The paper is organized as follows: in Section 2 a brief theory about the ultrasonic waveforms in wave guides is reported. In Section 3 the simulation algorithm, parameters and resulting waveforms are displayed. Section 4 reports the proposed method and Section 5 the experimental results. Finally the conclusions enclose the paper.

2 Theoretical basis

In this section the theoretical basis on wave propagation in elastic solids is briefly presented.

Let us consider an infinite medium. Two basic types of wave, dilatational and distortional, can propagate in an infinite medium, with each being characterized by a specific velocity. Furthermore, these wave types can exist independent from one another. A variety of terminology exists for the two wave types. Dilatational waves are also called irrotational and longitudinal waves. The distortional waves are also called equi-voluminal, rotational, torsional and shear waves.

The governing equation for an homogeneous isotropic elastic solid is represented by Navier's equation:

$$(\lambda + \mu)\nabla\nabla \cdot \mathbf{u} + \mu\nabla^2\mathbf{u} + \rho\mathbf{f} = \rho\ddot{\mathbf{u}} \quad (1)$$

where $\mathbf{u} = u_x\mathbf{e}_x + u_y\mathbf{e}_y + u_z\mathbf{e}_z$ is the displacement vector, λ and μ are the elastic constants for the material, that is the Lamé constants, ρ is the density, $\mathbf{f} = f_x\mathbf{e}_x + f_y\mathbf{e}_y + f_z\mathbf{e}_z$ is the vector of the body forces.

This equation is very complex but it is possible to obtain a simpler set of equations. For this purpose the scalar and vector potenzials Φ and \mathbf{H} are introduced. They are such that:

$$\mathbf{u} = \nabla\Phi + \nabla \times \mathbf{H}, \quad \nabla \cdot \mathbf{H} = 0 \quad (2)$$

In analogous way the scalar and vector potenzials f and \mathbf{B} for the vector \mathbf{f} are introduced:

$$\mathbf{f} = \nabla f + \nabla \times \mathbf{B}, \quad \nabla \cdot \mathbf{B} = 0. \quad (3)$$

With these positions the Navier's equation can be rewrite as follows:

$$\begin{aligned} (\lambda + 2\mu)\nabla^2\Phi + \rho\mathbf{f} &= \rho\ddot{\Phi} \\ \mu\nabla^2\mathbf{H} + \rho\mathbf{B} &= \rho\ddot{\mathbf{H}} \end{aligned} \quad (4)$$

The governing equations in the absence of body forces are:

$$(\lambda + \mu)\nabla\nabla \cdot \mathbf{u} + \mu\nabla^2\mathbf{u} = \rho\ddot{\mathbf{u}} \quad (5)$$

and:

$$\nabla^2\Phi = \frac{\rho}{\lambda + 2\mu}\ddot{\Phi} = \frac{1}{c_1^2}\frac{\partial^2\Phi}{\partial t^2} \quad (6)$$

$$\nabla^2\mathbf{H} = \frac{\rho}{\mu}\ddot{\mathbf{H}} = \frac{1}{c_2^2}\frac{\partial^2\mathbf{H}}{\partial t^2}$$

since $\mathbf{f} = \mathbf{B} = 0$. From the last equations it is possible to deduce c_1 and c_2 , the velocities of longitudinal and torsional waves respectively:

$$c_1 = \sqrt{\frac{\lambda + 2\mu}{\rho}} \quad (7)$$

$$c_2 = \sqrt{\frac{\mu}{\rho}} \quad (8)$$

These two velocities are related to the Poisson's coefficient ν as follows:

$$k = \frac{c_1}{c_2} = \sqrt{\frac{\lambda + 2\mu}{\mu}} = \sqrt{\frac{2 - 2\nu}{1 - 2\nu}} \quad (9)$$

from which it can be noted that it is always $c_1 > c_2$ since $0 \leq \nu \leq \frac{1}{2}$.

Consider now a solid cylindrical shell, like that used in tests of this work (figure 1).

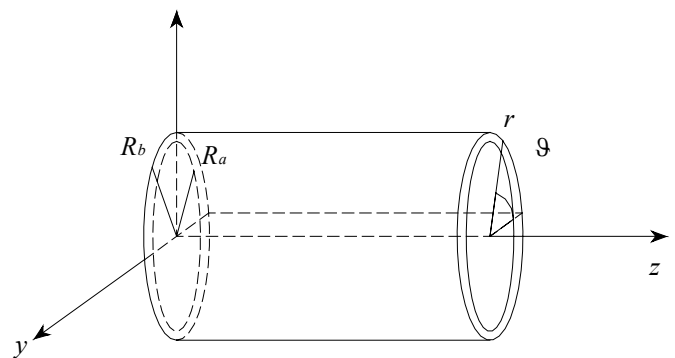


Fig.1 Cylindrical shell with both x, y, z and cylindrical coordinate systems.

For the analysis of wave propagation in cylindrical shell, the previous equations (1-9) still hold. However cylindrical coordinates are more appropriate here, and it is possible to write the displacement components as follows:

$$\begin{aligned} u_r &= \frac{\partial \Phi}{\partial r} + \frac{1}{r} \frac{\partial H_z}{\partial \vartheta} - \frac{\partial H_\vartheta}{\partial z} \\ u_\vartheta &= \frac{1}{r} \frac{\partial \Phi}{\partial \vartheta} + \frac{\partial H_r}{\partial z} - \frac{\partial H_z}{\partial r} \\ u_z &= \frac{\partial \Phi}{\partial z} + \frac{1}{r} \frac{\partial}{\partial r} (r H_\vartheta) - \frac{1}{r} \frac{\partial H_r}{\partial \vartheta} \end{aligned} \quad (10)$$

The stresses are given by Hooke's law $\tau_{ij} = \lambda \Delta \delta_{ij} + 2\mu e_{ij}$, where

$$\begin{aligned} e_{rr} &= \frac{\partial u_r}{\partial r}, \quad e_{\vartheta\vartheta} = \frac{1}{r} \frac{\partial u_\vartheta}{\partial \vartheta}, \quad e_{zz} = \frac{\partial u_z}{\partial z} \\ e_{r\vartheta} &= \frac{1}{2} \left(\frac{1}{r} \frac{\partial u_r}{\partial \vartheta} + \frac{\partial u_\vartheta}{\partial r} - \frac{u_\vartheta}{r} \right), \quad e_{rz} = \frac{1}{2} \left(\frac{\partial u_z}{\partial r} + \frac{\partial u_r}{\partial z} \right) \\ e_{\vartheta z} &= \frac{1}{2} \left(\frac{\partial u_\vartheta}{\partial z} + \frac{1}{r} \frac{\partial u_z}{\partial \vartheta} \right). \end{aligned} \quad (11)$$

and $\Delta \delta_{ij}$ is the deformation, with $i, j = r, z, \vartheta$.

In detail, for the problem presented in this work the boundary conditions on the stresses are:

$$\tau_{rr} = \tau_{r\vartheta} = \tau_{rz} = 0, \quad r = R_a, R_b, \quad (12)$$

where R_a and R_b are internal and external radii respectively.

Using equations 6, 10 and 12 it is possible determine the displacement components. It doesn't seem useful in this context to give the equations of the above mentioned displacements because of their complexity and length.

The general frequency equation results from the displacement equations, stress equations and boundary conditions. This equation includes several special propagation modes, such as torsional, longitudinal and flexural ones. The longitudinal mode involves only the displacements u_r and u_z and propagate dispersively. On the other hand, the torsional mode involves only the displacement u_ϑ and propagate non-dispersively [10]. The torsional mode has been excited in the simulations of the present work, it is described in the next section.

3 Simulation of ultrasonic waveform

The database used for this work is a collection of simulated waveforms.

The scattering of torsional waves in a cylindrical pipe with an asymmetric defect with respect to the axis of cylinder has been simulated. The parameters of the

simulation are resumed below. The pipe is made of steel 715, whose characteristics are in table 1. The geometric scheme of the test is described in table 2 and shown in figure 2. The pipe has not external covering and internal fluid and it is put in air. It has been chosen a torsional stress instead of a longitudinal one since it propagates only in the shell even when a fluid is present. The response of the defect to a longitudinal stress depends on the contrary also by the fluid, because it propagates both in the shell and fluid.

The excitation signal is shown in figure 3 and its parameters are resumed in table 3. It is a sinusoidal signal with frequency $f_0 = 55$ kHz, amplitude-modulate by an Hanning window with $N_h = 6$. When the excitation signal is applied, the first torsional mode propagates in the shell with a velocity $c_T = 3250$ m/s and a wavelength

Table 1. Characteristics of steel 715

Young's modulus	E	2.158e+11 N/m ²
Poisson's coefficient	ν	0.3
Density	ρ	7.84709e+3 kg/m ³
First Lamè constant	$\mu_L = E/2(1+\nu)$	8.3e+10 N/m ²
Second Lamè constant	$\lambda_L = \frac{\nu E}{(1+\nu)(1-2\nu)}$	1.245e+11 N/m ²
Velocity of longitudinal wave in an infinite media	$c_L = \sqrt{\frac{\lambda_L + 2\mu_L}{\rho}}$	6.084e+3 m/s
Velocity of shear wave in an infinite media	$c_T = \sqrt{\frac{\mu_L}{\rho}}$	3.252e+3 m/s
Thin plate velocity	$c_P = \sqrt{\frac{E}{(1-\nu^2)\rho}}$	5.497e+3 m/s
Bar velocity	$c_B = \sqrt{\frac{E}{\rho}}$	5.244e+3 m/s

Table 2. Geometric parameters of the test

Length L	L	4	m
Internal radius	R_a	4.5238e-2	m
External radius	R_b	5.0000e-2	m
Thickness	h	4.7620e-3	m
Medium radius	R	4.7619e-2	m
Ratio	h/R	0.1	
Plane of boundary condition	z_{bc}	0	m
Plane of defect axial location	z_{d0}	1	m
Observation plane	z_{obs}	0.6	m

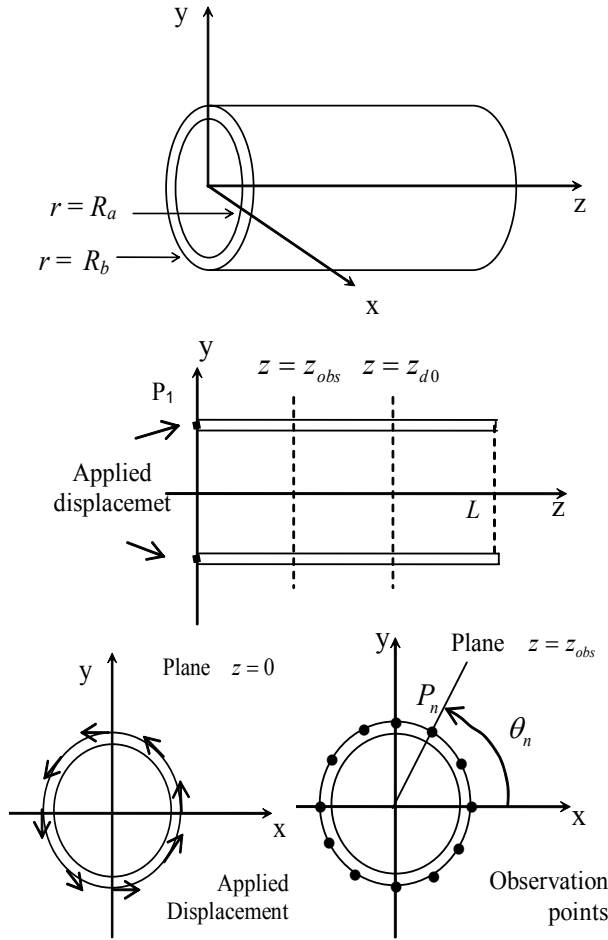


Fig. 2 Geometric scheme of the test

$\lambda = c_T / f_0 = 0.059 \text{ m}$. The excited mode does not depend on the coordinate ϑ and propagates non-dispersively. The higher order modes have a cut-off frequency higher than $f_0 = 55 \text{ kHz}$, so they can't propagate even if they are excited.

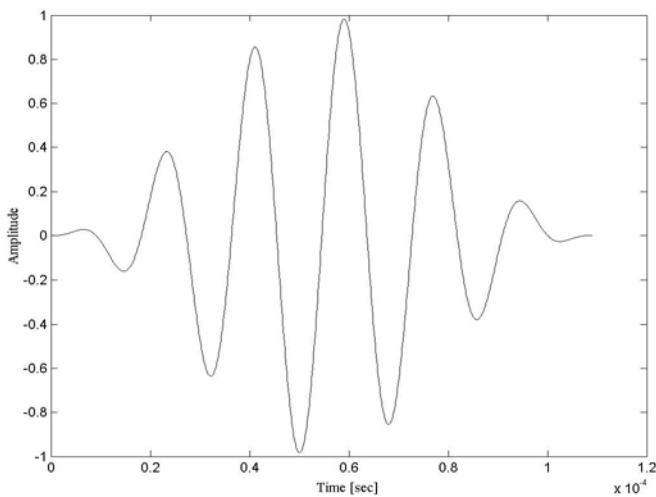


Fig. 3 The excitation signal $g_h(t)$

Table 3. Parameters of the excitation signal

Sinusoidal signal amplitude-modulate by an Hanning window			
Frequency	f_0	55	kHz
Amplitude	A	1	
Fundamental period	T_0	1.818×10^{-5}	s
Oscillations in the Hanning window	N_h	6	
Length of the excitation signal	$T_d = N_h T_0$	1.091×10^{-4}	s

The boundary condition is a “bcDisplacement” condition, that is a circumferential displacement over all the points of the external circumference that lays on the plane $z = 0$. If the displacement \mathbf{u} in cylindrical coordinates is referred as:

$$\mathbf{u} = u_r \mathbf{e}_r + u_\vartheta \mathbf{e}_\vartheta + u_z \mathbf{e}_z \quad (13)$$

it can be written for $z = 0$ and $r = R_b$:

$$\mathbf{u}(r, \vartheta, z; t) = \mathbf{u}(R_b, \vartheta, 0; t) = g_h(t) \mathbf{e}_\vartheta \quad (14)$$

where $g_h(t)$ is the excitation signal. There are 72 observation points which lay on the plane $z = z_{obs}$, uniformly distributed over the external circumference of the cylinder, they can be defined: $P_n \equiv (R_b, \vartheta_n, z_{obs})$, where $\vartheta_n = 0, 5, 10, \dots, 355 = (n-1) \cdot 5 \text{ deg}$ with $n = 1, 2, 3, \dots, 72$.

The defect is an external cavity. The geometric parameters of the defect are resumed in table 4. The defect simulates a corrosion of the external surface (see figure 4) of the pipes centered in the point $P_{d0} \equiv (R_{d0}, \vartheta_{d0}, z_{d0})$ with radial, angular and axial extensions. The radial extension of the corrosion is measured by the following parameter:

$$t_d \% = \frac{R_b - R_d}{R_b - R_a} \cdot 100 \quad (15)$$

with $R_a \leq R_d \leq R_b$, while $\Delta \vartheta_d$ and Δz_d denote angular and axial extension of the defect. As it can be seen from table 4, we have considered one value of radial extension and four values for angular and axial ones.

Because of the defect, a reflected wave and a transmitted one are generate in $z = z_{d0}$. If the defect is symmetric with respect to the axis, then these two waves are both torsional. On the other hand if the defect is asymmetric there are also longitudinal and flexural components of displacement. These components are due to the interaction between the incident torsional wave defect. In these tests an asymmetric defect with respect to the axis of the cylinder have been considered.

Table 4. Geometric parameters of the defects

Position	radial	R_{d0}	4.245	cm
	angular	θ_{d0}	180	deg
	axial	z_{d0}	1	m
Extension	radial	t_d	10	%
	angular	$\Delta\theta_d$	10, 20, 30, 40	deg
	axial	Δz_d	3, 12, 18, 24	mm

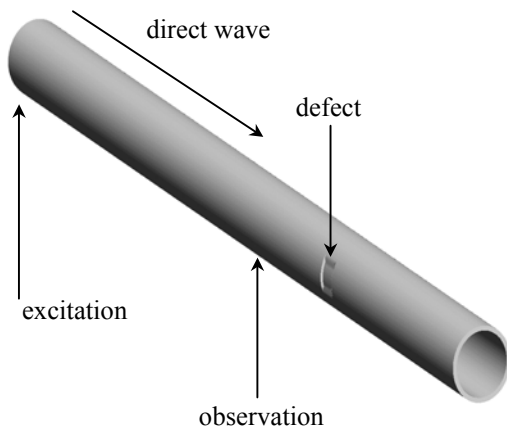


Fig. 4 Asymmetric defect with respect to axis

In figure 5 an example of direct wave, the wave reflected by the defect and that one transmitted through the defect, reflected by the end of pipe and transmitted again through the defect can be seen. The waves shown in figure are the normalized torsional components of the displacement observed in P_1 , the point that lays on the x positive semi-axis in $z = z_{obs}$.

Software CAPA 4.1 (WisSoft, Buckenhof, Germany) has been used to simulate the propagation of elastic waves in a cylindrical shell. This software employs a 3D finite elements method to simulate the propagation. The scattering of torsional wave for the following values of $(\Delta\theta_d; \Delta z_d)$ have been simulated, being fixed the radial extension of the defect: $(10;3), (20;12), (30;18), (40;24)$. Each simulation gives the components x, y, z of the displacement in each observation points. If it is necessary the radial and circumferential components can be deduced as follows:

$$\begin{aligned} u_r(P_n) &= u_x(P_n)\cos\mathcal{G}_n + u_y(P_n)\sin\mathcal{G}_n \\ u_\theta(P_n) &= -u_x(P_n)\sin\mathcal{G}_n + u_y(P_n)\cos\mathcal{G}_n \end{aligned} \quad (16)$$

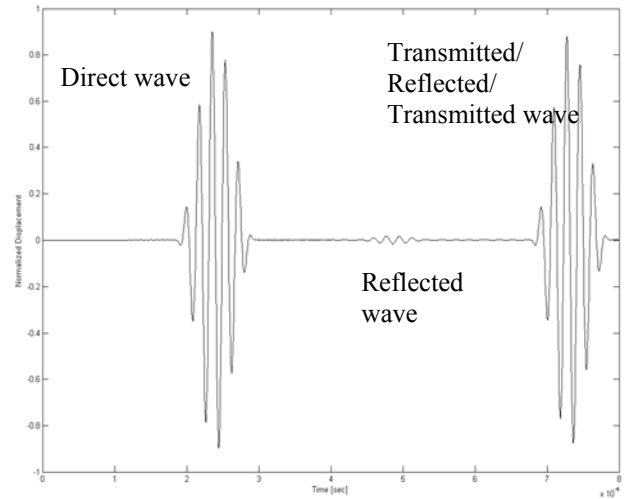


Fig. 5 Direct wave, wave reflected by the defect,

4 Overall approach

In this section the general approach to classify the defects on pipes is discussed and the experimental results by applying this method are shown.

A scheme of the proposed approach for classifying defects on pipes is shown in figure 6. The inputs of this system are the components x, y, z , of the wave reflected by a defect, the output is the classification of the defect. The steps of this approach are detailed in the following.

4.1 Feature extraction

The first step is the feature extraction. Timothy and Waag employed in [8] 69 parameters characterising waveforms. In this paper other two parameters are added to these (maximum absolute amplitude of waveform, maximum peak-to-peak amplitude of waveform) so a total of 35 time and 36 frequency domain features from each waveform have been calculated. All the parameters are listed in the Appendix.

4.2 Feature selection

In order to classify the ultrasonic waveform reflected by the defect it is useful to employ only the parameters which include the information about the characteristics of the various classes of defects. Therefore it is necessary to identify an efficient method to select the parameters that give a good class discrimination. With this aim the k -nearest neighbour algorithm is used, to select a subset of waveform features which better represent the information on the defect. This subset contains the features which make the lower errors in k -nn classification. In other words each single feature is used to classify the defects by means of k -nn and an optimal subset features consists of those with the best recognition rate. The figure 7 shows as an example the errors made in classifying the waveforms of the component y in the four classes of defects mentioned in the previous section. It can be seen that for some parameters the error is lower than 50%, while it is larger than 75% for others,

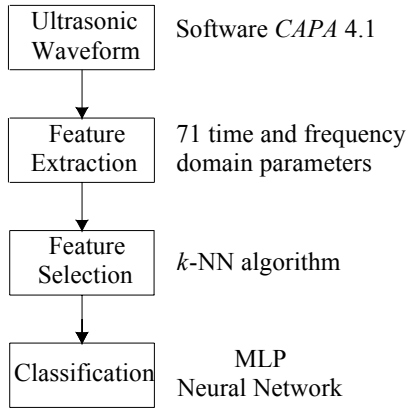


Fig. 6 Scheme of the proposed approach

particularly high errors for the frequency domain parameters can be noted. This behaviour is similar to every components of the displacement, and it could be due to the very small bandwidth of the simulated waveforms. Moreover, the waveform of the component y are better classified than the others, since there is a larger number of parameters which make low errors. This means that the component y contains more information on the defect than others.

Another problem is the correct number of the parameters which have to form the optimal subset; it will be the input vector for the neural classifier that performs the final diagnosis. This is a problem of optimal threshold identification. The choice of a value for this threshold allows to divide the set of parameters in two subsets. The parameters which make an error lower or equal than the threshold constitute the optimal subset. Furthermore the threshold value represents the maximum acceptable percent error made by a single parameter in classifying a defect. A low value of the threshold means few parameters which make low errors in classifying defects, but too few parameters could not form a set with a sufficient

information for the final classifier. On the other hand an high value of threshold means to consider also parameters which make high errors. In this case there is the risk of having a poor quality information for the final classification. In this work it has been found that a good compromise is a value of the threshold which leads to form a subset of parameters about 15.

4.3 Neural classifier

The last step of the presented approach is the classification. In this step the vectors of the optimal features associated with the waveforms feed an MLP neural network. Each waveform is classified according to the value of neural network outputs. The defect class is given by the neuron with the maximum output. In the next section this result is described in detail [11].

5 Experimental results

A database of $72 \times 4 = 288$ waveforms for each component of the displacement has been analyzed, where 72 is the number of the observation points, and 4 are the values of $(\Delta \mathcal{G}_d; \Delta z_d)$ as quoted in Section 2; in fact the radial extension of the defect is fixed.

The 71 time and frequency domain parameters for each waveform of the database have been evaluated. Then the k -nearest neighbour algorithm selects the subset of waveform features which make the lower errors in classifying defects. The better results have been obtained with an optimal number of neighbours $k = 4$ and the y component waveforms of the displacement. For the other components of the displacement the same number of parameters is obtained but for higher values of the threshold. For this reason, it is possible to assert that the y component of displacement characterizes the defect better than the others. This means that it is possible to find a sufficient number of parameters which make errors lower or equal than a suitable threshold characterizing the defects. In this case the 14 parameters whose errors are lower or equal than the threshold 0,55 (figure 7) have been found. They are here listed:

- Maximum absolute amplitude of the waveform;
- Maximum peak-to-peak amplitude of the waveform;
- Global pulse duration between 25% levels;
- Local fall time from peak to 25% level;
- Local rise variance between 25% level and peak;
- Local fall variance between peak and 25% level;
- Local fall variance between peak and 50% level;
- Global rise variance between 25% level and peak;
- Global rise variance between 50% level and peak;
- Global fall variance between peak and 25% level;
- Global fall variance between peak and 50% level;
- Local rise variance between 25% level and peak of spectrum;

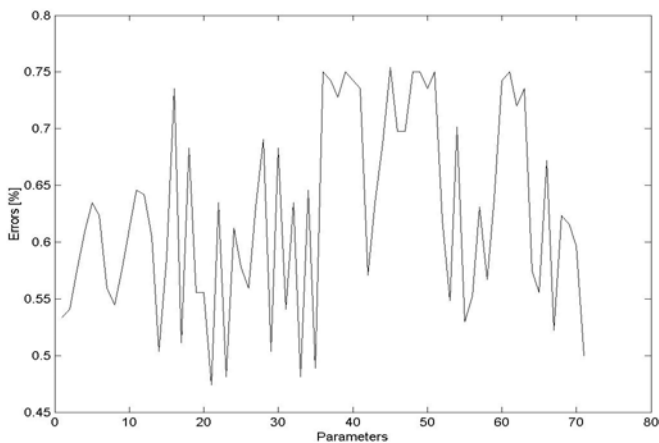


Fig. 7 Error of each parameter in classifying the waveform of the component y

- Local rise variance between 50% level and peak of spectrum;
- Global rise variance between 50% level and peak of the spectrum.

The above mentioned parameters form the input vector for the final classifier. It is a supervised Multi Layer Perceptron (MLP) neural network with a sigmoid activation function and a back-propagation learning. The neurons of the hidden layer are 21, while there are 4 output neurons since 4 classes of defects have been analyzed.

An input vector is classified in the j -th class ($j = 1,2,3,4$) when the j -th output value is maximum. The class to which an input vector I belongs is therefore defined as follows:

$$c(I) = \{j \text{ if } u_j = \max_k(u_k) \quad k = 1, \dots, 5\} \quad (17)$$

where u_j is the j -th output value.

Since only the y component waveforms of the displacement have been processed, the input set is a 14×288 matrix, whose columns are the 14 parameters vectors associate to each waveform reflected by the defect. This input set has been divided into two subsets: a training set constituted by 230 vectors and a validation set constituted by the remaining 58 vectors. In table 5 the vectors of the validation set split in the four classes are reported.

The performance of the proposed classifiers has been evaluated in term of recognition rate. It is defined as the ratio between the number of vectors correctly classified and the total amount of the processed vectors. In the tests of this work the recognition rate of the neural classifier is 96,7%.

5 Conclusions

The main target of non-destructive techniques is the automatic identification of defects on industrial products or engineering materials as accurately as possible. However, the non-destructive testing processes are often difficult and depend significantly on the experience of the tester. In this paper an automatic method to help the decision step of human operators about the corrosion level of tubes has been presented, so our approach can be very useful to forecast out of orders and avoid them. The method was based on the ultrasonic inspection of non-reachable pipes and exploits the neural network ability to classify flaws of various size on the pipes. A suitable number of time and frequency features extracted by the ultrasonic signal feeds the neural network. These features constitute an optimal feature set to characterize the ultrasonic waveform. The results show that defects with different dimensions can be correctly identified and may be used as class reference to evaluate the state of the pipes, even if the recognition rate quickly decreases when the demanded accuracy increases. Future works will be devoted to overcome this drawback, in order to improve

the classification and recognize the dimensions of more large variety of defects.

Appendix

1. Maximum absolute amplitude of waveform.
2. Mean value of the normalized waveform amplitude values.
3. Variance of the normalized waveform amplitude values.
4. Maximum peak-to-peak amplitude of the waveform.
5. Difference between 50% level and 25% level (waveform CD).
6. Difference between 75% level and 25% level (waveform CD).
7. Difference between 90% level and 25% level (waveform CD).
8. Local pulse duration between 25% levels.
9. Global pulse duration between 25% levels.
10. Mean value of the normalized envelope function.
11. Variance of the normalized envelope function.
12. Local rise time from 25% level to peak.
13. Local rise time from 50% level to peak.
14. Local fall time from peak to 25% level.
15. Local fall time from peak to 50% level.
16. Local rise slope between 25% level and peak.
17. Local rise variance between 25% level and peak.
18. Local rise slope between 50% level and peak.
19. Local rise variance between 25% level and peak.
20. Local fall slope between peak and 25% level.
21. Local fall variance between peak and 25% level.
22. Local fall slope between peak and 50% level.
23. Local fall variance between peak and 50% level.
24. Global rise time from 25% level to peak.
25. Global rise time from 50% level to peak.
26. Global fall time from peak to 25% level.
27. Global fall time from peak to 50% level.
28. Global rise slope between 25% level and peak.
29. Global rise variance between 25% level and peak.
30. Global rise slope between 50% level and peak.
31. Global rise variance between 50% level and peak.
32. Global fall slope between peak and 25% level.
33. Global fall variance between peak and 25% level.
34. Global fall slope between peak and 50% level.
35. Global fall variance between peak and 50% level.
36. Difference between 50% level and 25% level (spectrum CD).
37. Difference between 75% level and 25% level (spectrum CD).
38. Difference between 90% level and 25% level (spectrum CD).
39. Frequency of the maximum value of the power spectrum.
40. Center frequency of the power spectrum.
41. Measured bandwidth.
42. Mean value of the normalized power spectrum.
43. Variance of the normalized power spectrum.
44. Fraction of total power between lower 25% level and peak.
45. Fraction of total power between lower 50% level and peak.
46. Fraction of total power between peak and upper 25% level.
47. Fraction of total power between peak and upper 50% level.
48. Local rise frequency from 25% level to peak.
49. Local rise frequency from 50% level to peak.
50. Local fall frequency from peak to 25% level.
51. Local fall frequency from peak to 50% level.
52. Local rise slope between 25% level and peak of spectrum.
53. Local rise variance between 25% level and peak of spectrum.
54. Local rise slope between 50% level and peak of spectrum.
55. Local rise variance between 50% level and peak of spectrum.
56. Local fall slope between peak of spectrum and 25% level.
57. Local fall variance between peak of spectrum and 25% level.
58. Local fall slope between peak of spectrum and 50% level.
59. Local fall variance between peak of spectrum and 50% level.
60. Global rise frequency between 25% level and peak of spectrum.
61. Global rise frequency between 50% level and peak of spectrum.

62. Global fall frequency between peak of spectrum and 25% level.
63. Global fall frequency between peak of spectrum and 50% level.
64. Global rise slope between 25% level and peak of spectrum.
65. Global rise variance between 25% level and peak of spectrum.
66. Global rise slope between 50% level and peak of spectrum.
67. Global rise variance between 50% level and peak of spectrum.
68. Global fall slope between peak of spectrum and 25% level.
69. Global fall variance between peak of spectrum and 25% level.
70. Global fall slope between peak of spectrum and 50% level.
71. Global fall variance between peak of spectrum and 25% level.

CD = cumulative distribution.

Acknowledgments

The authors thank the research unit of Prof. M. Raugi, Dipartimento di Sistemi Elettrici e Automazione, University of Pisa, for providing the simulation data obtained by means of the software CAPA.

This work was partly supported by the Ministero dell'Università e della Ricerca Scientifica and partly by the Politecnico di Bari.

References:

- [1] Y. H. Kim, S. Song, J. Y. Kim, A new technique for the identification of ultrasonic flaw signal using deconvolution, *Ultrasonics*, Vol.41, 2004, pp. 799-804.
- [2] J. L. Rose, J. Barshinger, Using Ultrasonic Guided Wave Mode Cutoff for Corrosion Detection and Classification, *IEEE Ultrasonics Symposium*, 1998, pp. 851-854.

- [3] F. Bettayed, T. Rachedi, H. Benbartaoui, An improved automated ultrasonic NDE system by wavelet and neuron networks, *Ultrasonics*, Vol.42, 2004, pp. 853-858.
- [4] F. W. Margrave, K. Rigas, D. A. Bradley, P. Barrowcliffe, The use of neural networks in ultrasonic flaw detection, *Measurements*, Vol.25, 1999, pp. 143-154.
- [5] G. Simone, F. C. Morabito, R. Polikar, P. Ramuhalli, L. Udpa, S. Udpa, Feature extraction techniques for ultrasonic signal classification, *International Journal of Applied Electromagnetics and Mechanics*, Vol.15, 2001/2002, pp. 291-294.
- [6] R. Wendel, J. Dual, Application of networks to quantitative non-destructive evaluation, *Ultrasonics*, Vol.34, 1996, pp. 461-465.
- [7] V. Khandetsky, I. Antonyuk, Signal processing in defect detection using back-propagation neural networks, *NDT&E International*, Vol.35, 2002, pp. 483-488.
- [8] T. J. Case, R. C. Waag, Flaw Identification from Time and Frequency Features of Ultrasonic Waveforms, *IEEE Transactions on Ultrasonics, and Frequency Control*, Vol.43, No. 4, 1996, pp. 592-600.
- [9] R. Draï, M. Khelil, A. Benchaala, Time frequency and wavelet transform applied to selected problems in ultrasonics NDE, *NDT&E International*, Vol.35, 2002, pp. 567-572.
- [10] K. F. Graff, *Wave motion in elastic solids*, Dover, 1991.
- [11] S. Haykin, *Neural Networks: a comprehensive foundation*, Prentice Hall, 1999.